NUCL SCI TECH (2018) 29:149
https://doi.org/10.1007/s41365-018-0484-z

Radiation dose detection using a high-power portable optically stimulated luminescence real-time reading system

Yi-Hang Wang[1] · Hua Chen[1] · Fei Chen[1] · Yong-Gang Yuan[1] · Tai-Ping Peng[1]

Received: 16 November 2017 / Revised: 29 April 2018 / Accepted: 13 May 2018 / Published online: 5 September 2018

Abstract Optically stimulated luminescence (OSL) reading systems are becoming smaller and capable of real-time detection. To improve real-time and multipurpose radiation dosimetry readings, we built a real-time continuous-wave (RCW) OSL reading system. This system is both small and lightweight, and it employs powerful laser excitation (478 mW/cm^2) at the dosimetry probe location. We investigate the possibility of using the RCW mode to read the radiation luminescence (RL) or OSL by using a single-crystal Al_2O_3:C dosimeter in a low-dose-rate ^{137}Cs γ field. Our results indicate that the RL/OSL follows a stable and uniform distribution. The minimum detected doses associated with the RL, OSL, and RL + OSL signals are 2.1×10^{-2}, 3.17×10^{-1}, and 5.7×10^{-2} μGy, respectively. This device provides a framework for the future development of applications for practical radiation dose measurements.

Keywords OSL · Real-time reading · Al_2O_3:C · Radiation dose

This work was supported by the International Fusion Reactor Experiment Program (No. 2014GB112004).

✉ Tai-Ping Peng
ptp4205@sina.com

[1] Institute of Nuclear Physics and Chemistry, Chinese Academy of Engineering Physics, Mianyang 621900, China

1 Introduction

Optically stimulated luminescence (OSL) is a technology that uses laser stimulation in a pre-irradiated material that emits a luminescence signal proportional to the radiation dose. The suitability of OSL for radiation dosimetry was discovered by Albrecht and Mandeville [1] in 1955. Its development was further improved when Akselrod and McKeever [2] used a pulsed OSL mode to read dosimetry signals. OSL detectors have gradually become a valuable competitor to conventional thermoluminescence dosimetry (TLD) systems, whose main application is passive radiation dosimetry. Al_2O_3:C-based OSL dosimetry systems have started to replace TLD systems as personal dosimetry devices at a number of leading, nationally accredited service providers, and already meet the American National Standards Institute criteria [3]. OSL has also been used in personal dosimetry systems in other countries [4]. Applications of OSL range from radiotherapy [5–9] to environmental monitoring [10, 11], space (astronaut) dosimetry [12], and geological research [13].

The idea of coupling OSL to optical fibers for remote, real-time radiation dose monitoring [14–17] has been studied by several research groups. OSL devices are also becoming smaller and capable of real-time measurements. At Landauer Inc., OSL dosimeter tests were developed by Jursinic [18], who aimed to make the device even more compact. Their device proved to have significant advantages over TLD systems and diodes for in vivo dosimetry and routine clinical dose measurements. Liu [19] developed an OSL reading system integrated into an optical fiber dosimeter, which can perform online radiation dose measurements. However, its counting method was not truly real time but rather similar to that of conventional OSL systems. Marckmann et al. [20] designed an OSL real-time system using a small cylindrical (diameter × length = 0.5 mm × 2 mm) Al_2O_3:C crystal as a dosimetry probe. It is small enough for in vivo dosimetry. However, a beam splitter was employed in that configuration to separate the excitation light from the stimulated light, which increased the design difficulty. Furthermore, the optical fiber probe was attached to the detector by an optical fiber, which does not permit changing of the detector material.

In this paper, we introduce a novel home-built integral real-time continuous-wave (RCW) OSL reading system. In this small and lightweight device, the optical fiber arrangement increases the luminescence signal and improves the signal-to-noise ratio. The dosimeter probe structure ensures compatibility with different luminescent materials. We also investigate the possibility of using Al_2O_3:C as an online OSL material for real-time dose measurements. This paper describes three types of signals that characterize the radiation dose. We used radiation luminescence (RL) and OSL signals in combination with this real-time optical luminescence reading system. A simple algorithm is introduced to calibrate the luminescence signals with the radiation dose. This results in high accuracy and enables assessment of the dose delivered to the point of measurement using real-time information.

2 Hardware and experimental

2.1 Hardware

The measurements were taken with a home-built real-time OSL reading system. A schematic diagram and a photograph of the light-tight box are shown in Fig. 1.

As shown in Fig. 1a, the primary optical component of the OSL reading system consists of a green laser diode, a photomultiplier tube (PMT), a counter (ORTEC Model 871), a dosimeter probe, a fiber coupler, an optical filter (Hoya-B-370), and a transmission fiber. Figure 1b shows an overview of the RL/OSL readout system. All the electrical and optical components are commercially available, and all the optical components, except for the dosimeter probe and counter, are contained in a light-tight box. An electrical wire is connected to the controller readout, and a long fiber-optic cable is connected to the dosimeter probe. This light-tight box is small, and its light weight allows easy storage and transport.

Stimulation light at 532 nm is provided by a laser diode, which has a power density of 478 mW/cm^2 at the detection material location. The laser transmitted through the central optical fiber is collected at the dosimeter probe, and a stimulated luminescence light peak at 420 nm appears, which is attributed to the F center. There is guide back to the light-tight box through six surrounding optical fibers to the PMT. A 395–440 nm band-pass filter is used to exclude the reflected stimulating light. The PMT–filter combination has its peak sensitivity at 420 nm. This is optimal for collection of the stimulated luminescence and exclusion of the reflected stimulating light. One advantage of this design lies in the transmitting optical fiber, which creates the light path shown in Fig. 2a. The emitted light is transported through six surrounding optical fibers, which enhances the luminescence signal and improves the signal-to-noise ratio. This arrangement also reduces the circuit design difficulty. The PMT output is connected to the outer counter, which displays the number of counted photons.

A photograph of the dosimeter probe is shown in Fig. 2b. The dosimetric material and optical fiber are coupled within the dosimeter probe, which is mounted at the end of a 1.8-m-long fiber-optic cable. The probe and the

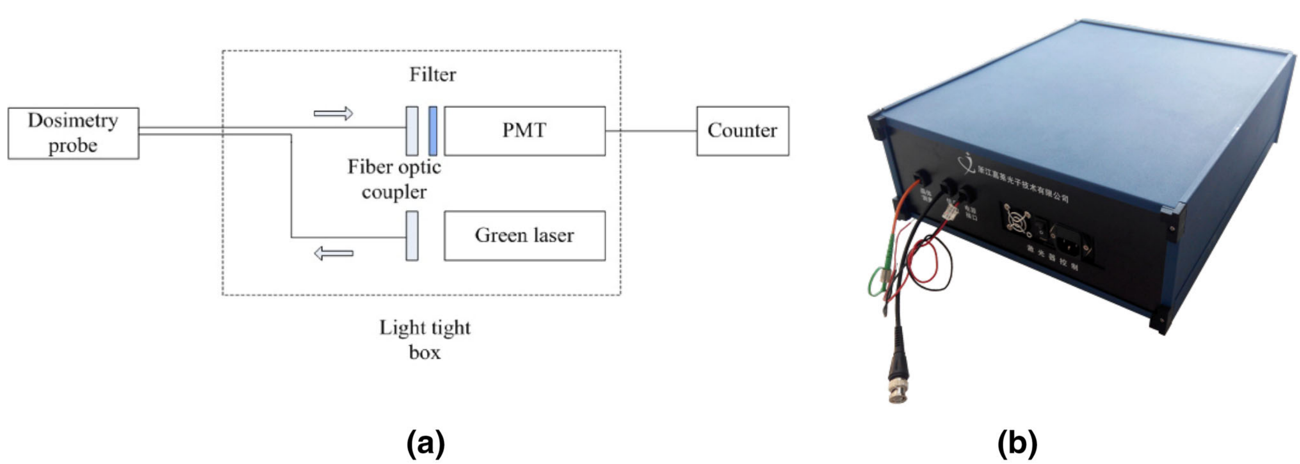

Fig. 1 **a** Schematic of the real-time RL/OSL readout system and **b** photograph of the light-tight box (45 × 40 × 15 cm^3, 11 kg)

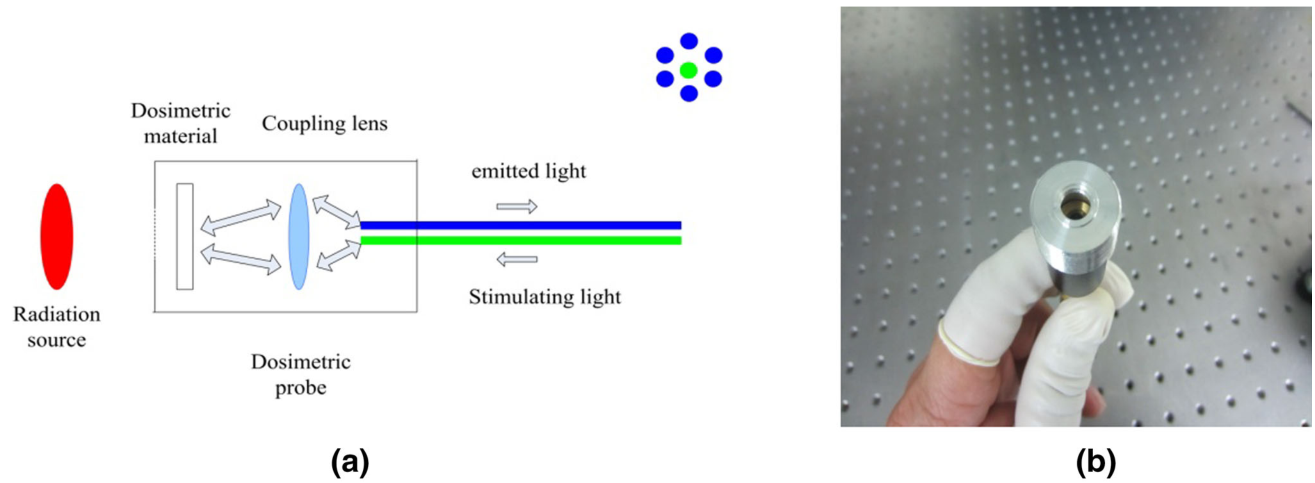

Fig. 2 **a** Schematic and **b** photograph of dosimeter probe (Color online)

inside of the lid are shiny, so they reflect the laser and luminescence to increase the power density of both. The flexible fiber allows the probe to be installed at arbitrary locations and access complicated radiation environments while ensuring the safety of the operator. The structure of the probe allows for easy replacement of the dosimetric material and is suitable for different types of material. This device would be appropriate for measuring a low-dose-rate radiation source (below a few hundred micrograys per hour), and the high-power optical stimulation source (478 mW/cm^2) can effectively exclude trapped electrons in the dosimetric materials.

2.2 Experimental design

Irradiation was performed with a calibrated low-dose-rate ^{137}Cs γ source. The dosimetry probe was placed near the open gate of the lead pot that contained the ^{137}Cs source. The dose rate at the dosimetry probe position was calibrated at 3.81×10^2 μGy/h using a portable γ dose rate meter (BH3103A). A single crystal of aluminum oxide doped with carbon (Al_2O_3:C), provided by the Shanghai Institute of Optics and Fine Mechanics (Chinese Academy of Sciences), was used as the dosimetric material. The dimensions of the crystal were 5 mm $\times$ 4 mm $\times$ 1 mm, and optical transparency was obtained after double-sided polishing. A 30-min photobleaching treatment was carried out before the experiment using a 420-nm blue light beam. The radiation monitor probes were placed within the ^{137}Cs γ radiation field to measure the exposure dosage. All experiments were performed at room temperature.

The Al_2O_3:C material exhibits light emission during irradiation or upon stimulation by another light source after irradiation. A simplified scheme of the relevant physical principles is presented in Fig. 3. When the material is exposed to ionizing radiation, electron–hole pairs are created. These ionized electrons can enter the conduction band and decay via trapping centers that offer possibilities for both nonradiative and radiative transitions. To determine the dose, we use the radiative transitions. In other words, we detect a signal associated with a certain wavelength emitted by the material. When the material is placed in the radiation field and emits luminescence immediately, it behaves like a scintillator, emitting light in the form of RL. This process involves trapping of an ionized electron by a shallow trap, where the electron is unstable and is eventually released back to the conduction band. Subsequently, it can be trapped by other deeper traps or luminescence centers. The ionized electrons trapped in deeper traps have lower energy levels, which are stable and do not contribute to the RL process. These electrons are stored there for a long time. When stimulated by light with a suitable wavelength after irradiation, these trapped electrons are released and reabsorbed in traps or luminescence centers. When they recombine at luminescence centers, the emitted light is called the OSL signal. Both RL and OSL emission contain short and long luminescence components.

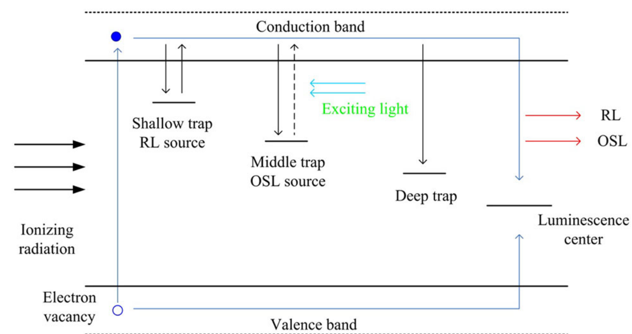

Fig. 3 Simple band gap model of the RL and OSL processes

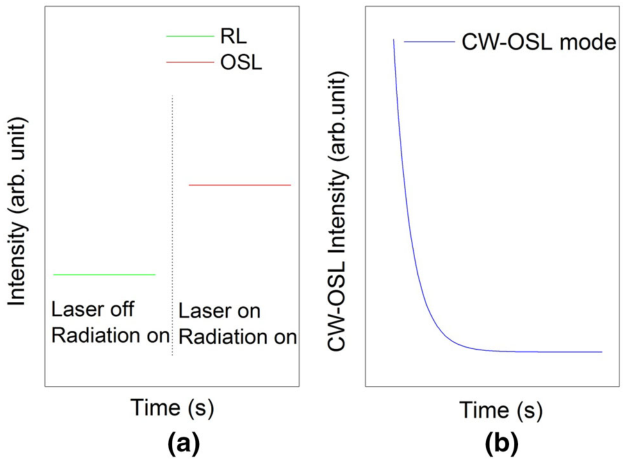

Fig. 4 Schematics of **a** the reading mode and **b** the routine CW-OSL mode

Figure 4 compares the properties of the two types of emission in our experiment. The RL depends strongly on the properties of the incoming radiation. If the exposure is interrupted using very fast signal attenuation, the RL stops immediately. Conversely, the OSL signal is maintained until the electrons trapped in the deeper defect sites all exit under the excitation light, even though the radiation source is closed. Both signals can be used for radiation dose measurements. In this study, independent absorbed dose estimates were obtained by integrating either the complete RL signal during irradiation or the complete OSL signal stimulated by the stimulating light during irradiation. The reading modes for the RL and OSL are shown as green and red lines in Fig. 4a, respectively. This is different from the conventional CW-OSL mode [3, 21] shown in Fig. 4b. This method can be called a really continuous-wave OSL system, where the radiating material is constantly stimulated by a constant-intensity light source, and the OSL signal is monitored continuously throughout the stimulation period. The radiation and optical stimulation are performed at the same time, not sequentially, and the radiation source has a low dose rate, but the optical stimulation source has a high power density (478 mW/cm^2). Thus, the trapped electrons can be effectively excluded, so there is no accumulation of trapped electrons in the dosimetry material, and the stored dose is not saturated. Consequently, there are no changes in the sensitivity of the Al_2O_3:C material. Because the radiation dose signal is calculated as the area under the continuous-wave intensity curve, this method is called the integral RCW-OSL method.

The strength of both signals (RL and OSL) depends on the background level and includes the stem effect [22], which is unwanted light emission from the fiber cable during irradiation, plus the contribution from the equipment/sample background, which interacts with the radiation pattern. The background signal was removed by simple subtraction, along with the interference from the stem effect and radiation pattern. A diagram showing the signal strength relationships among the RL, OSL, stem effect, and equipment/sample background is displayed in Fig. 5. The remaining RL and OSL signal strength is almost constant with time; see Fig. 7.

Next, the experimental data are fitted with a straight line, and the area under each line is calculated as a function of time. This integral corresponds to the time evolution of the total counts during a time interval. Because the radiation dose is correlated with the radiation time, this provides the trend for the total counts as a function of the radiation dose.

2.3 Minimum detectable dose (MDD)

The minimum detectable dose (MDD) of a detector system is affected by the signal-to-noise ratio. The noise depends on the standard deviation of the noise signal. Another important factor is the sensitivity of the detection system to the desired signal. Here, the dose signal is calculated as the area under the RCW signal according to the RCW-OSL method discussed above. We can therefore determine the MDD using a method developed by Rawat et al. [23], which uses the integrated area under the CW-OSL wave, according to the following equation:

$$\mathrm{MDD}(\mu\mathrm{Gy}) = \frac{3\sigma(\mathrm{counts})}{\text{Integrated CW-OSL signal per unit dose at given } \Phi\ (\mathrm{counts}/\mu\mathrm{Gy})},$$

where σ is the standard deviation of the background noise counts for the integration time t, 3σ indicates that the MDD is evaluated within a 99.7% confidence level, and Φ stands for the stimulation intensity in mW/cm^2. In our experiment, the noise and RL/OSL signals are almost constant over time. Hence, the standard deviation (σ) of the background noise counts was calculated during a relatively long period (2 min). The integration time can be chosen freely, as long

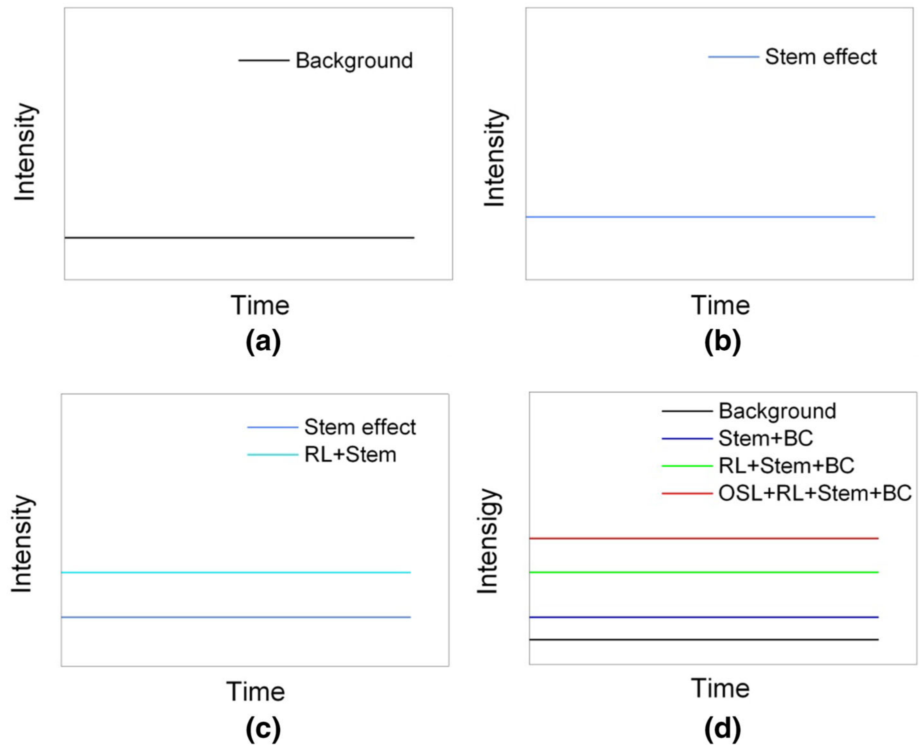

Fig. 5 Diagram of the signal strength relationships among the different signals as a function of time: **a** background (BC) signal, **b** stem effect signal, **c** signal strength, stem effect, and RL + Stem signal, **d** signal strength and background, Stem + BC, RL + Stem + BC, OSL + RL + Stem + BC signal (Color online)

as the background signal is subtracted from it. The stimulated power Φ used in this study is 478 mW/cm^2.

The noise signal contains several components, which can be measured separately. We assume that the noise components are mutually independent, so the standard deviations (σ) of each component satisfy the following relations:

$$\sigma = \sqrt{D}, \tag{1}$$

$$RL = RL' - b1, \tag{2}$$

$$D(RL) = D(RL') + D(b1), \tag{3}$$

$$S = b' - b, \tag{4}$$

$$D(S) = D(b') + D(b), \tag{5}$$

$$BCosl = b2 + RL + S = b2 + RL' - b1 + b' - b, \tag{6}$$

$$D(BCosl) = D(b2) + D(RL') + D(b1) + D(b') + D(b). \tag{7}$$

Here, $b1$ is the noise signal of the stem effect and the equipment in the radiation field (without illumination, without a crystal sample, with radiation); RL' is the RL signal of the crystal samples before the noise signal is subtracted (without illumination, with crystal samples, with radiation); RL is the net RL signal of the crystal sample; b is the noise signal of the equipment (with illumination, without radiation, without crystal samples); b' is the noise signal of the equipment (with illumination, without radiation, with crystal samples); S is the noise signal of the crystal samples caused by the illumination; $b2$ is the noise signal of the stem effect and the equipment in the radiation field (with illumination, without crystal samples, with radiation); and $BCosl$ is the total OSL background signal of the crystal samples during normal operation (with illumination, with radiation). D is the variance of these signal data; because we assume that the different signals are mutually independent, the variance of the total signal can be calculated by adding those of each component.

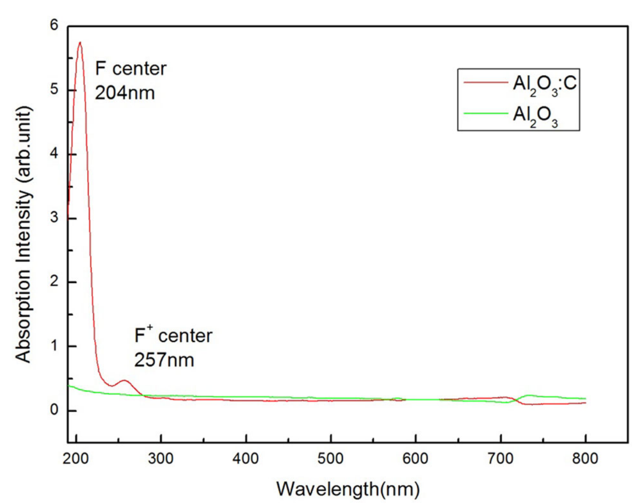

Fig. 6 Absorption intensity of an Al_2O_3:C single crystal and an Al_2O_3 single crystal (Color online)

3 Results and discussion

During laser stimulation, luminescence is observed in the irradiated sample because trapped electrons are delocalized and recombined at luminescence centers. This unique luminescence property is found in very few materials, and the most well-known of which is Al_2O_3:C. Figure 6 shows the optical absorption spectrum of an Al_2O_3:C single crystal, together with that of an Al_2O_3 single crystal for reference. The measuring equipment was a SolidSpec-3700. Although the undoped Al_2O_3 single crystal shows no clear absorption peaks across the entire tested range, the Al_2O_3:C single crystal shows a strong absorption band at 204 nm and a weaker absorption band at 257 nm. Both the location and shape of these absorption bands are consistent with other research results [24–26], confirming the suitability of our Al_2O_3:C crystal for use as a dosimetric material. The 204-nm absorption peak is caused by F centers, which correspond to electron transitions from the 1S level to the 1P level [27]. The main luminescence signal at 410 nm is also emitted from this center [27–29], whereas the 257-nm peak is caused by F^+-center absorption, which corresponds to electron transitions from the 1A level to the 1B level [30]. These results indicate the important role of C in the formation of an effective luminescence center.

Figure 7 shows a time series of the RL and OSL counts, which were acquired with a time step of 1 s period over a total time of 8 h. The interval time between each period and excitation laser to stimulate the OSL is constant. The background signal has already been subtracted from the values displayed in the graph. The trends of both the RL and OSL are constant over time. The average value of these data points does not change with time under these conditions. Therefore, average-value curves can be used to represent the mean values of the RL and OSL counts. The average values for the RL and OSL counts are 1.56×10^2 counts/s and 6.7×10^1 counts/s, respectively. Overall, the entire data set can be fitted by a straight line, with the data points evenly distributed on both sides. In other words, the RL and OSL counts do not change with time but maintain an almost constant average value when the stimulating light is off and on, respectively. This phenomenon is different from the results obtained by Polf et al. [31], who used a high dose rate ranging from 10 to 34 mGy/s with beta particles as the radiation source. In another study [30], the experimental curve of counts over time showed an initially increasing trend that reached saturation. It took longer to reach equilibrium than we found in this study. In our test, we used a lower dose rate of 3.81×10^2 μGy/h and a gamma-ray radiation source, which led to a different accumulation effect. The different results may be due in part to the different radiation source, and the time required to reach equilibrium is probably influenced by the radiation dose rate. The continuous high-power exciting laser can effectively remove the accumulated dose over time under this low-dose-rate condition, which makes the average

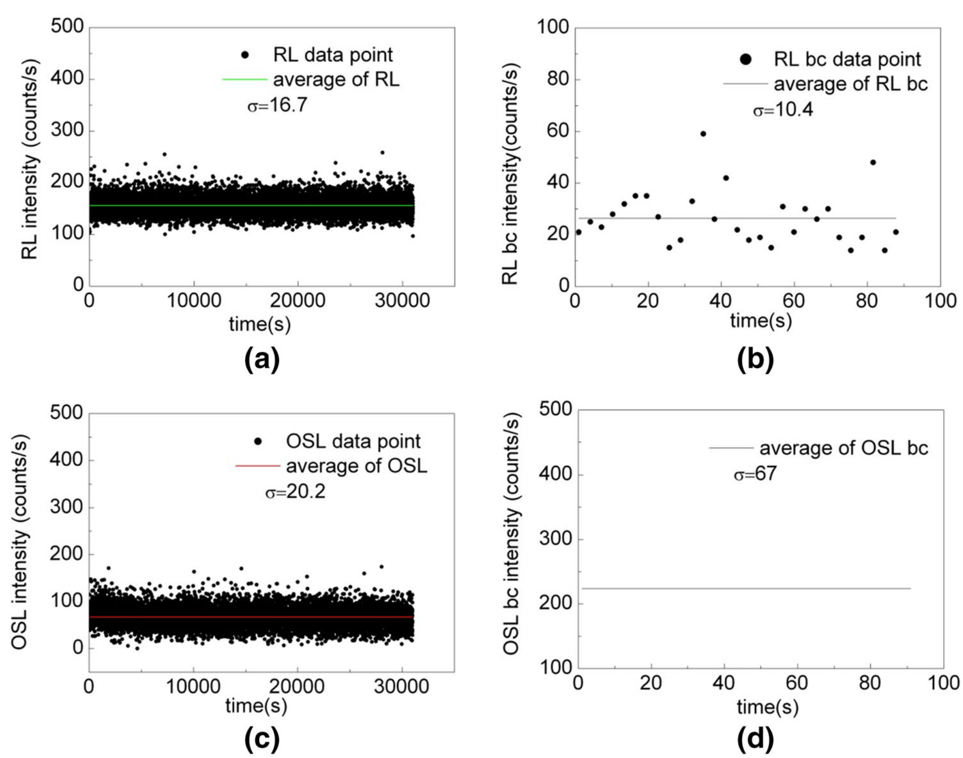

Fig. 7 RL and OSL counts. **a** RL counts over 8 h, **b** RL background signal for 2 min, **c** OSL counts over 8 h, **d** average OSL background signal for 2 min

luminescence signal suitable for many types of low-dose-rate radioactive source monitoring in real time.

Figure 7b, d displays the background signals of the RL and OSL counts, respectively. The background of the RL can be measured in a single operation. Therefore, we can obtain a simple description of the data point itself. Conversely, the background of the OSL consists of several components that must be measured separately. Therefore, it is not easy to display it in Fig. 7d. The standard deviation is calculated by considering all the effects discussed in the previous sections. We can deduce that the average values of the RL and OSL counts can be expected to remain constant for a virtually infinite time under these radiation and excitation light conditions. This result allows us to develop a simple radiation dose algorithm using the RL/OSL signal.

Now we find the relationship between the radiation dose and the equipment readout. The radiation dose can be calculated from the radiation time using the calibrated value of 3.81×10^2 μGy/h from the ^{137}Cs source. The total counts of the RL/OSL signals can be found by calculating the areas under the average-value curves for a given time. Figure 8 shows the total count–dose curves of the RL and OSL signals. The graph shows a linear correlation between the total counts and the radiation dose. Because the integration was performed using the average values of the RL and OSL counts, the curve shape is expected to remain the same if the total count–dose curve is extended indefinitely. This relation is consistent with previous research results on OSL, which, however, showed a saturating dose limit. This is because the conventional CW-OSL reading mode excites the material using a laser after irradiation, so the dose is saturated after a long radiation time. Conversely, no saturation effect is observed in the RCW-OSL reading mode. The reason may be the strong excitation power density of 478 mW/cm^2, which continuously excites trapped electrons away from defect centers.

Next, the MDD is calculated for these radiation and measuring conditions. When the RL counts are used as the characteristic radiation dose, σ is 16.7, and the integrated counts per μGy are 2385.7, so the MDD is 2.1×10^{-2} μGy, whereas in the case of the OSL counts, the MDD is 3.17×10^{-1} μGy.

In our reading mode (RCW-OSL), RL and OSL are emitted simultaneously. In order to further improve the signal-to-noise ratio and reduce the MDD, an attempt is made to combine the RL and OSL counts to characterize the radiation dose. Figure 9a shows that the total RL + OSL counts are also uniformly located near the average-value curve, which can thus be used to index all the data points. This result is in agreement with the individual RL and OSL counts. Figure 9b displays the RL + OSL total count–dose curve, which has a larger slope than the RL and OSL dose–response curves. However, it can be extended for an indefinite time as well. For the RL + OSL counts, the minimum detectable dose is 5.7×10^{-2} μGy. Although the net effective signal increases, the standard deviation of the background signal interferes with the OSL background, which moves the MDD to an intermediate value between the RL and OSL values.

A conventional CW-OSL reading process was also performed with our RCW-OSL reading system. Our dosimeter probe was inserted into the radiation field for 1 h without illumination. Then, the dosimeter probe was exposed to the exciting laser to read the luminescence signal in the routine CW-OSL mode. Figure 10 shows the count attenuation curve, which reveals exponential decay toward the background level after 2 min with no plateau at the beginning. This indicates that there is no saturation effect after 1 h of exposure. The attenuation coefficient is

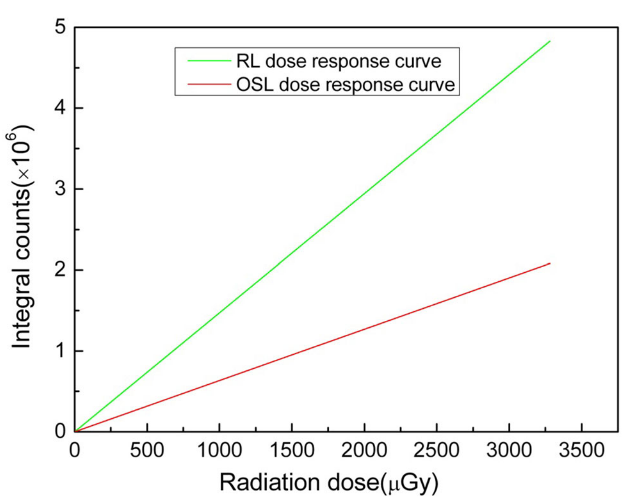

Fig. 8 Count–dose curves of RL and OSL (Color online)

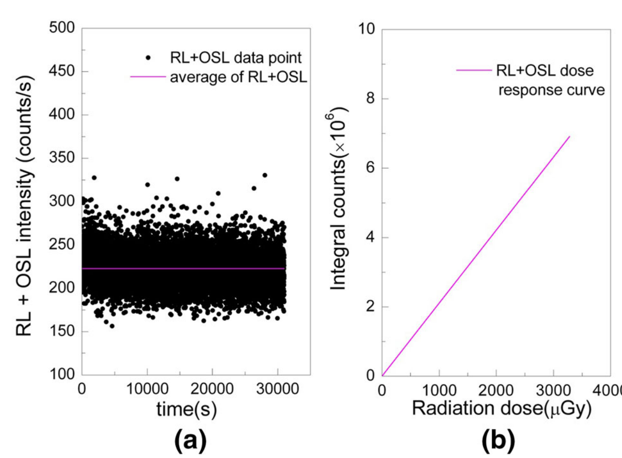

Fig. 9 Combined RL + OSL **a** counts versus time and **b** total counts versus dose (Color online)

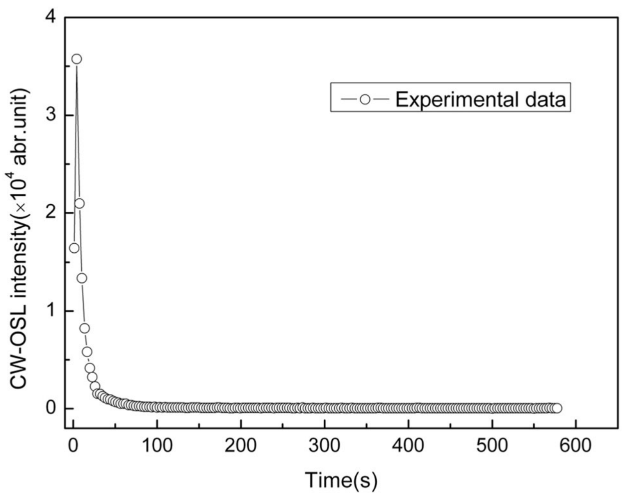

Fig. 10 Counts versus time, where the dosimetry detector was read using the conventional CW-OSL mode after an irradiation time of 1 h

influenced by both the experimental conditions and the material properties of the dosimeter. This signal also includes short- and long-duration components, and the curve's shape is in agreement with other results from the literature. The curve exhibits a sharp peak during the first few seconds; this is caused by the laser opening time, which cannot be accurately controlled. This means that the actual laser opening time occurred during the first second, when the counter was counting. The first count is 16,406, and the second count is 35,764; the number of counts in the first second should be much larger than this value. However, this error can be corrected to achieve a higher degree of accuracy. This demonstrates that our home-built RCW-OSL reading system can also effectively work using the conventional CW-OSL mode.

Exposure of an Al_2O_3:C single crystal exposed to sunlight for one day resulted in a luminescence signal. This means that sunlight can erase the radiation dosimetric information and generate new dosimetric information for this detector material. This phenomenon has been previously reported by West et al. [32]. In the RCW-OSL mode, when the radiation source is closed and the exciting green light is on, the OSL decreases abruptly, soon approaching the background level. This indicates that the reading laser itself (478 mW/cm^2) can effectively bleach the remaining luminescence centers, although a small amount of the long luminescence component remains. To clear these signals completely before reusing the device, a separate 420 nm blue light photobleaching process should be used.

4 Conclusion

A home-built RL/OSL dosimetric real-time reading system (RCW-OSL system) was developed, which can measure the radiation dose over a long time in a low-dose-rate ^{137}Cs γ field. The equipment is compact and lightweight, making it easy to carry and suitable for monitoring a stationary radiation source such as the ^{137}Cs source used in this paper. The optical fiber structure and dosimetry probe design can help improve the signal-to-noise ratio, enhance the power density (478 mW/cm^2), and enable simple changes in the detection material. A simple radiation dose algorithm was developed, which uses the average values to quantify the RL/OSL signal and determine the MDDs of the RL signal, OSL signal, and RL + OSL signal, whose experimental values were 2.1×10^{-2}, 3.17×10^{-1}, and 5.7×10^{-2} μGy, respectively. This fast algorithm can be easily used to determine the radiation dose. Future work will be focused on studying the dose-rate dependence and evaluating real-time monitoring of charged particle radiation doses. Through continuous improvement, this system may be used to obtain a real-time radiation dose meter suitable for a wide range of applications.

Acknowledgements The authors would like to thank the ZheJiang Jia Lai photon technology company for assembling this reading system and providing the picture and reference structure diagram shown in this paper.

References

1. H.O. Albrecht, C.E. Mandeville, Storage energy in BeO. Phys. Rev. **101**, 1250 (1956). https://doi.org/10.1103/PhysRev.101.1250
2. M.S. Akselrod, S.W.S. McKeever, A radiation dosimetry method using pulsed optically stimulated luminescence. Radiat. Prot. Dosim. **81**, 167–175 (1999). https://doi.org/10.1093/oxfordjournals.rpd.a032583
3. L. Botter-Jensen, S.W. McKeever, A.G. Wintle, *Optically stimulated luminescence* (Elsevier Science: BV Publication, Amsterdam, 2003)
4. S.Y. Lee, K.J. Lee, Development of a personal dosimetry system based on optically stimulated luminescence of α-Al_2O_3:C for mixed radiation fields. Appl. Radiat. Isot. **54**, 675–685 (2001). https://doi.org/10.1016/S0969-8043(00)00302-X
5. I. Mrčela, T. Bokulić, J. Izewska et al., Optically stimulated luminescence in vivo dosimetry for radiotherapy: physical characterization and clinical measurements in ^{60}Co beams. Phys. Med. Biol. **56**, 6065–6082 (2011). https://doi.org/10.1088/0031-9155/56/18/018
6. M.C. Aznar, C.E. Andersen et al., Real-time optical-fibre luminescence dosimetry for radiotherapy: physical characteristics and applications in photon beams. Phys. Med. Biol. **49**, 1655–1669 (2004). https://doi.org/10.1088/0031-9155/49/9/005
7. L.F. Nascimento, F. Vanhavere, E. Boogers et al., Medical dosimetry using a RL/OSL prototype. Radiat. Meas. **71**, 359–363 (2014). https://doi.org/10.1016/j.radmeas.2014.05.028

8. C.J. Marckmann, C.E. Andersen et al., Optical fibre dosemeter system for clinical applications based on radioluminescence and optically stimulated luminescence from Al_2O_3:C. Radiat. Prot. Dosim. **120**, 28–32 (2006). https://doi.org/10.1093/rpd/nci506
9. S. Magne, S. Deloule, A. Ostrowsky et al., Fiber-coupled, time-gated Al_2O_3:C radioluminescence dosimetry technique and algorithm for radiation therapy with LINACs. IEEE Trans. Nucl. Sci. **60**, 2998–3007 (2013). https://doi.org/10.1109/TNS.2013.2263640
10. A.F. Fernandez, B. Brichard, S. O'Keeffe et al., Real-time fibre optic radiation dosimeters for nuclear environment monitoring around thermonuclear reactors. Fusion Eng. Des. **83**, 50–59 (2008). https://doi.org/10.1016/j.fusengdes.2007.05.034
11. D.M. Klein, E.G. Yukihara, S.W.S. Mckeever et al., In situ long-term monitoring system for radioactive contaminants. Radiat. Prot. Dosim. **119**, 421–424 (2006). https://doi.org/10.1093/rpd/nci604
12. E.G. Yukihara, G.O. Sawakuchi, S. Guduru et al., Application of the optically stimulated luminescence (OSL) technique in space dosimetry. Radiat. Meas. **41**, 1126–1135 (2006). https://doi.org/10.1016/j.radmeas.2006.05.027
13. J. Walling, Optically stimulated luminescence dating of fluvial deposits: a review. Boreas **31**, 303–322 (2010). https://doi.org/10.1111/j.1502-3885.2002.tb01076.x
14. A.R. Beierholm, R.O. Ottosson, L.R. Lindvold et al., Characterizing a pulse-resolved dosimetry system for complex radiotherapy beams using organic scintillators. Phys. Med. Biol. **56**, 3033–3045 (2011). https://doi.org/10.1088/0031-9155/56/10/009
15. T. Teichmann, J. Sponner, C. Jakobi et al., Real time dose rate measurements with fiber optic probes based on the RL and OSL of beryllium oxide. Radiat. Meas. **90**, 201–204 (2016). https://doi.org/10.1016/j.radmeas.2016.01.015
16. R.R. Patil, R. Barve, S.V. Moharil et al., Development of Ag doped crystalline SiO_2 for possible application in real-time in vivo OSL dosimetry. Radiat. Meas. **71**, 208–211 (2014). https://doi.org/10.1016/j.radmeas.2014.02.009
17. C.E. Andersen, J.M. Edmund, S.M.S. Damkjar, Precision of RL/OSL medical dosimetry with fiber-coupled Al_2O_3:C influence of readout delay and temperature variations. Radiat. Meas. **45**, 653–657 (2010). https://doi.org/10.1016/j.radmeas.2009.11.047
18. P.A. Jursinic, Characterization of optically stimulated luminescent dosimeter, OSLDs, for clinical dosimetric measurements. Med. Phys. **34**, 4594–4604 (2007). https://doi.org/10.1118/1.2804555
19. Y.P. Liu, Z.Y. Chen, W.Z. Bai et al., A study on the real-time radiation dosimetry measurement system based on optically stimulated luminescence. Chin. Phys. C **32**, 381–384 (2008). https://doi.org/10.1088/1674-1137/32/5/011
20. C.J. Marckmann, C.E. Andersen, M.C. Aznar et al., Optical fibre dosemeter systems for clinical applications based on radioluminescence and optically stimulated luminescence from Al_2O_3:C. Radiat. Prot. Dosim. **120**, 28–32 (2006). https://doi.org/10.1093/rpd/nci506
21. S.W.S. McKeever, Optically stimulated luminescence dosimetry. Nucl. Instrum. Methods Phys. Res. B **184**, 29–54 (2001). https://doi.org/10.1016/S0168-583X(01)00588-2
22. R. Gaza, S.W.S. McKeever, M.S. Akselrod, Near-real-time radiotherapy dosimetry using optically stimulated luminescence of Al_2O_3:C mathematical models and preliminary results. Med. Phys. **32**, 1094–1102 (2005). https://doi.org/10.1118/1.1884365
23. N.S. Rawat, B. Dhabekar, M.S. Kulkarni et al., Optimization of CW-OSL parameters for improved dose detection threshold in Al_2O_3:C. Radiat. Meas. **71**, 212–216 (2014). https://doi.org/10.1016/j.radmeas.2014.02.013
24. X.B. Yang, H.J. Li, Q.Y. Bi et al., Growth of α-Al_2O_3:C crystal with highly sensitive optically stimulated luminescencce. J. Lumin. **129**, 566–569 (2009). https://doi.org/10.1016/j.jlumin.2008.12.015
25. M.S. Kulkarni, D.R. Mishra, K.P. Muthe et al., An alternative method of preparation of dosimetric grade α-Al_2O_3:C by vacuum-assisted post-growth thermal impurification technique. Radiat. Meas. **39**, 277–282 (2005). https://doi.org/10.1016/j.radmeas.2004.03.005
26. M.S. Akselrod, V.S. Kortov, D.J. Kravetsky et al., Highly sensitive thermoluminescent anion-defect α-Al2O3: C single crystal detectors. Radiat. Prot. Dosim. **33**, 119–122 (1990). https://doi.org/10.1093/oxfordjournals.rpd.a080715
27. K.H. Lee, J.H. Crawford, Luminescence of the F center in sapphire. Phys. Rev. B **19**, 3217–3221 (1979). https://doi.org/10.1103/PhysRevB.19.3217
28. K.P. Muthe, M.S. Kulkarni, N.S. Rawat et al., Melt processing of alumina in graphite ambient for dosimetric applications. J. Lumin. **128**, 445–450 (2008). https://doi.org/10.1016/j.jlumin.2007.09.013
29. M.G. Rodriguez, G. Denis, M.S. Akselrod et al., Thermoluminescence, optically stimulated luminescence and radioluminescence properties of Al_2O_3:C:Mg. Radiat. Meas. **46**, 1469–1473 (2011). https://doi.org/10.1016/j.radmeas.2011.04.026
30. B.D. Evans, M. Stapelbroek, Optical properties of the F^+ center in crystalline Al_2O_3. Phys. Rev. B **18**, 7089 (1978). https://doi.org/10.1103/PhysRevB.18.7089
31. J.C. Polf, S.W.S. McKeever, M.S. Akselrod et al., A real-time, Fibre optic dosimetry system using Al_2O_3 fibres. Radiat. Prot. Dosim. **100**(1–4), 301–304 (2002). https://doi.org/10.1093/oxfordjournals.rpd.a005873
32. W.G. West, K.J. Kearfott, S.M. Bernal, The sunlight OSL response of a commercially available α-Al_2O_3:C personnel dosimetry material. Radiat. Prot. Dosim. **119**, 344–349 (2006). https://doi.org/10.1093/rpd/nci691